Flow Reversals in Thermally Driven Turbulence

Kazuyasu Sugiyama,[1,3] Rui Ni,[2] Richard J. A. M. Stevens,[1] Tak Shing Chan,[1,2] Sheng-Qi Zhou,[2] Heng-Dong Xi,[2] Chao Sun,[1,2] Siegfried Grossmann,[4] Ke-Qing Xia,[2] and Detlef Lohse[1,*]

[1]*Physics of Fluids Group, Faculty of Science and Technology, Impact and MESA+ Institutes & Burgers Center for Fluid Dynamics, University of Twente, 7500AE Enschede, The Netherlands*

[2]*Department of Physics, The Chinese University of Hong Kong, Shatin, Hong Kong, China*

[3]*Department of Mechanical Engineering, School of Engineering, The University of Tokyo, Tokyo, Japan*

[4]*Fachbereich Physik, Renthof 6, D-35032 Marburg, Germany*

(Received 18 March 2010; published 16 July 2010)

We analyze the reversals of the large-scale flow in Rayleigh-Bénard convection both through particle image velocimetry flow visualization and direct numerical simulations of the underlying Boussinesq equations in a (quasi-) two-dimensional, rectangular geometry of aspect ratio 1. For medium Prandtl number there is a diagonal large-scale convection roll and two smaller secondary rolls in the two remaining corners diagonally opposing each other. These corner-flow rolls play a crucial role for the large-scale wind reversal: They grow in kinetic energy and thus also in size thanks to plume detachments from the boundary layers up to the time that they take over the main, large-scale diagonal flow, thus leading to reversal. The Rayleigh vs Prandtl number space is mapped out. The occurrence of reversals sensitively depends on these parameters.

DOI: 10.1103/PhysRevLett.105.034503 PACS numbers: 47.27.−i

Spontaneous flow reversals occur in various buoyancy driven fluid dynamical systems, including large-scale flows in the ocean, the atmosphere, or the inner core of stars or the Earth, where such reversals are associated with the reversal of the magnetic field. The paradigmatic example for buoyancy driven flow is the Rayleigh-Bénard system, i.e., a fluid-filled cell heated from below and cooled from above; see, e.g., the recent reviews [1,2]. In this system flow reversals have been detected and statistically analyzed, mainly through measurements of the temperature at one [3] or several points [4,5] in the flow or at the walls and more recently through flow visualization with particle image velocimetry (PIV) [6,7]. Various models have been developed to account for the reversals, either of stochastic nature [8,9] or based on simplifying (nonlinear) dynamical equations [10,11], which show chaotic deterministic behavior. Most of the experimental studies have so far been done in a cylindrical cell, where the complicated three-dimensional dynamics of the convection role (see, e.g., [12,13] and Sec. VIII of [1]) complicates the identification of the reversal process.

In the present Letter, we restrict ourselves to the study of flow reversals in (quasi-) two-dimensional (2D) rectangular geometry: experimentally to Rayleigh-Bénard (RB) convection in a flat cell and numerically to direct numerical simulations (DNS) of the two-dimensional Oberbeck-Boussinesq equations, for which reversals have been observed already in [14]. This approach offers three advantages: (i) The flow reversal in quasi-2D is less complicated than in 3D (and therefore, of course, may be different); (ii) the visualization of the full flow is possible; and (iii) a study of a considerable fraction of the Rayleigh number Ra vs Prandtl number Pr phase space becomes numerically feasible.

The experiments were made in rectangular, quasi-2D cells [15]. To extend the range of Ra, two cells of nearly identical geometry are used. The larger (smaller) cell has a horizontal cross section of 24.8×7.5 (12.6×3.8) cm^2, and the height of the larger (smaller) cell is $H =$ 25.4 cm ($H = 12.6$ cm), giving an aspect ratio $\Gamma \approx 1$ in the plane of the main flow (and an aspect ratio of about 0.3 in the direction perpendicular to it). The fluid is water with a mean temperature of 28 °C, corresponding to $\mathrm{Pr} = 5.7$. For direct visualization of flow reversals, PIV is used for a few selected Ra. The PIV measurement in this system has also been described previously [15]. To study the statistical properties of the reversals over long time periods, we measure the temperature contrast δT between two thermal probes embedded, respectively, in the left and right sides of either the top or the bottom plates. Reversals of the upward going hot plumes and downward going cold plumes correspond to the switching between the right and left sides of the system, δT therefore is indicative of reversals.

The numerical code is based on a fourth-order finite-difference discretization of the incompressible Oberbeck-Bousinesq equations and has been described in [16]. The grid resolution has been chosen according to the strict requirements as formulated in [17]. As in experiment also the numerical flow is wall bounded, i.e., we use no-slip boundary conditions at all solid boundaries: $\mathbf{u} = \mathbf{0}$ at the top ($z = H$) and bottom ($z = 0$) plates as well as on the side walls $x = 0$ and $x = H$. For the temperature at the side walls heat-insulating conditions are employed and $T_b - T_t = \Delta$ is the temperature drop across the whole cell.

Times are given in multiples of the large eddy turnover time t_E, defined by $t_E := 4\pi/\langle|\omega_c(t)|\rangle$, where ω_c denotes the center vorticity.

We start by showing qualitative features of the reversal process using examples from both numerical simulations and experiments. Figure 1 shows snapshots of the temperature and velocity fields from DNS and those of the velocity field from experiment just before, during, and after the large convection roll reversal. Corresponding videos can be viewed from the supplementary materials [18]. Visually, the reversal process can be easily detected. To automatize this we measure the local angular velocity at the center of the cell; however, with this method some plumes passing through the center can lead to erroneous reversal counting. A better way is to rely on a global quantity, e.g., the global angular momentum (which has been successfully used for reversal characterization in 2D Navier-Stokes turbulence [16,19]). This is defined as $L(t) = \langle -(z - H/2)u_x(\boldsymbol{x}, t) + (x - H/2)u_z(\boldsymbol{x}, t)\rangle_V$, where $\langle \ldots \rangle_V$ represents averaging over the full volume. The time dependence of L from simulation and experiment, as shown, respectively, in Figs. 1(d) and 1(h), indeed nicely reveals the reversal through a sign change.

From the movies corresponding to Fig. 1 [18] the basic role of the corner flows in the reversal process can be observed: While the main roll is diagonally orientated in the cell, smaller counterrotating rolls develop in diagonally opposing corners. They are energetically fed by detaching plumes from the boundary layers (BL) trapped in the corner flows, leading to their growth. Once the two corner flows have reached a linear extension of $\approx H/2$ [Fig. 1(b) and moment (b) in Figs. 1(d) and 1(f) and moment (f) in Fig. 1(h)], they destroy the main convection roll and establish another one circulating in the opposite direction.

The heights $h(t)$ of the corner flows are measured by first fitting the temperature profile at the respective sidewall with splines, and then identifying the position of the steepest gradient of $T(z)$: From movies and snapshots we judge that this is an excellent measure for the height $h(t)$ of the corner flow. Time series of $h(t)$, together with the (rescaled) center vorticity $\omega_c(t)$ as quantitative measure of the strength of the large-scale convection roll, are shown in Fig. 2. It is seen that after a reversal [as indicated by a sign change in $\omega_c(t)$] the respective corner flow grows roughly linearly in time, before it reaches the half-height $h(t)/H \approx 1/2$ and breaks down, leading to flow reversal. However, the growth of the corner flow need not always lead to a reversal of the large-scale convection roll: There are cases in which the corner flow loses energy due to some plume detachment from it, leading to full recovery of the large-scale convection roll in its original direction (e.g., at

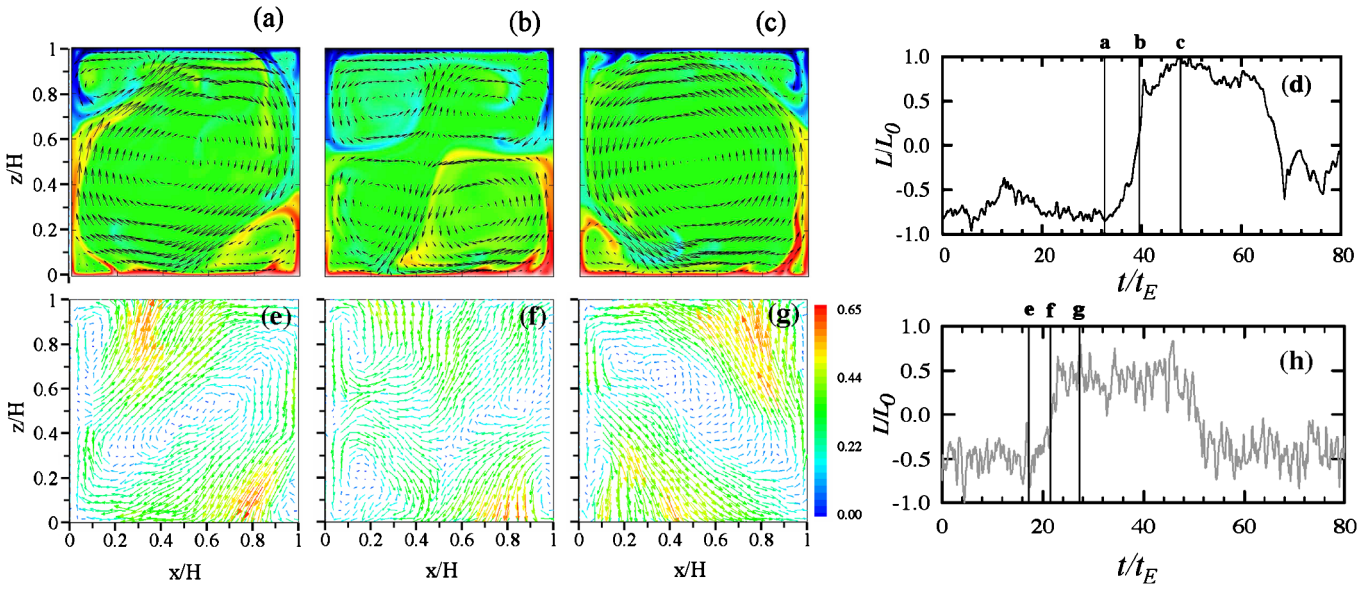

FIG. 1 (color online). Top panel: Snapshots of the temperature (color) and velocity (arrows) field and time trace of angular momentum from numerical simulations ($\mathrm{Ra} = 10^8$ and $\mathrm{Pr} = 4.3$). Bottom panel: Snapshots of the velocity field and time trace of angular momentum from experiment ($\mathrm{Ra} = 3.8 \times 10^8$ and $\mathrm{Pr} = 5.7$). (a), (b), and (c) show the instantaneous dimensionless temperature $(T - T_t)/\Delta$ distribution. (d) shows the temporal change of the dimensionless angular momentum $L(t)/L_0$, where L_0 is the maximum of the absolute value of L. The positive and negative signs indicate the anticlockwise and clockwise circulations, respectively. (e), (f), and (g) show the PIV-measured instantaneous velocity field and (h) the normalized instantaneous angular momentum $L(t)/L_0$. The color bar indicates the magnitude of the velocity (in unit of cm/sec). The snapshots in (a), (b), and (c) give numerical, and those in (e), (f), and (g) give experimental examples of the large-scale circulation before, during, and after a reversal process, as indicated in (d) and (h), respectively. Note that (b) and (f) show clearly the key role played by the growth of the corner rolls in the reversal process. Corresponding movies are offered in the supplementary material [18].

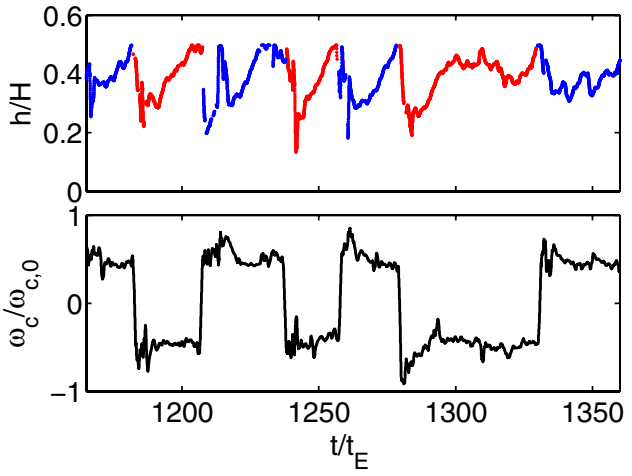

FIG. 2 (color online). Time series of the center vorticity $\omega_c(t)$ (rescaled by its maximum) (lower panel) and the heights $h(t)$ of the lower left [blue (above positive ω_c)] and right [red (above negative ω_c)] corner flows, revealing their approximate linear growth. Not all growth processes need to lead to an immediate successful reversal, as seen for $t/t_E \approx 1300$. Ra $= 10^8$, Pr $=$ 4.3.

$t/t_E \approx 1300$ in Fig. 2). Also in experiment we have observed such unsuccessful buildups of the corner flow. Below we will try to quantify the energy gains and losses of the corner flows.

The mean time interval $\langle\tau\rangle$ between successive reversals is shown in Fig. 3. First, we clearly see that experiment and simulation are in very good agreement. The figure shows that $\langle\tau\rangle/t_E$ at most weakly depends on Ra up to Ra $\approx 2 \times 10^8$, but for larger Ra rapidly increases with increasing Ra, i.e., reversals occur less and less frequently. The numbers

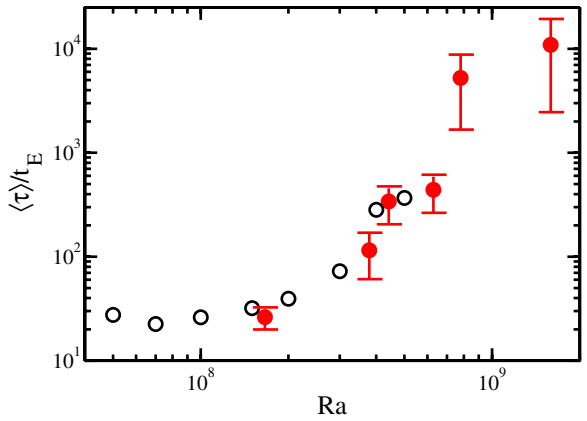

FIG. 3 (color online). Log-log plot of the Ra dependence of the mean time intervals $\langle\tau\rangle$ between successive reversals, normalized in terms of the large eddy turnover time t_E. Filled symbols are from experiment and open symbols from simulation. The error bar originates from the statistics of the reversals; for the numerical case it is smaller than the symbol size.

mean that there are only very few reversals: of order one per hour in the Ra $\sim 10^8$ range down to one within two days in the Ra $\sim 10^9$ range. For Ra $\geq 5 \times 10^8$ no reversals could be detected any more in our numerical simulations, even for an averaging time of 2600 large eddy turnovers (see accompanying movie [18]). In experiment two reversals could still be observed at Ra $= 1.6 \times 10^9$ (presumably due to the longer observation time in experiment which goes beyond 10 000 large eddy turnovers, corresponding to four days), but these also cease for larger Ra.

These findings led us to map out a considerable fraction of the Ra-Pr parameter space. The results for both the simulations and the experiments are shown in Fig. 4. One sees a rather complicated structure. But given the limited amount of data, experiment and simulation are in general agreement, especially considering the fact that the simulations are for the true 2D case whereas the experiments run in a quasi-2D cell. It should again be pointed out that the experimental data point with the highest Ra ($= 1.6 \times 10^9$) that still shows a reversal has an extremely low reversal rate (0.5/day), which corresponds to waiting for ~5500 large-scale turnover time for a single reversal to occur.

From Fig. 4 we conclude that not only for too large Ra (as compared to above case of Fig. 1 with Ra $= 10^8$ and Pr $= 4.3$) the reversals do not occur any more, but also for too large or too small Pr. How to physically understand this complicated behavior? The key towards an understanding lies, from our point of view, in the role of the corner flows, and is based on a detailed observation of many movies at various Ra and Pr (see accompanying material [18]). As

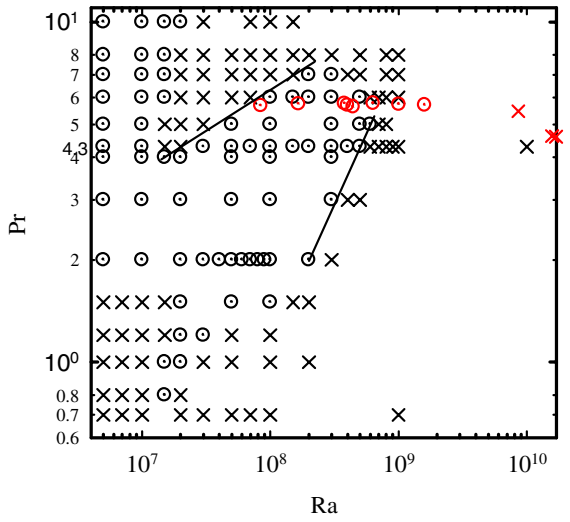

FIG. 4 (color online). Phase diagrams in the Ra-Pr plane. Red symbols (which are the symbols with $5 <$ Pr<6) are from experiment and the black ones from DNS. Circles correspond to detected reversals [23], crosses to no detected reversals, in spite of excessive simulation (or observation) time. The straight lines are guides to the eye; they have (from left to right) slopes 0.25 and 1.00.

stated above, the corner-flow rolls are fed by plumes detaching from the plates' boundary layers. For too small Pr (i.e., too large thermal diffusivity) the thermal energy they carry is lost through thermal diffusion. On the other hand, for too large Pr (i.e., too large kinematic viscosity) the thermal BL is nested in the kinematic BL and the thermal coupling of the corner flow towards the thermal BL is hindered. In both cases the buildup of the corner flow and thus the reversals are suppressed. The situation is similar to the one in rotating RB, where Ekman vortices form, sucking heat out of the thermal BL and enhancing the heat flux. Also here there is an optimal Pr ≈ 10 for which the Nusselt number is maximal, and for larger or smaller Pr the very same above mechanisms hinder efficient heat transport [20].

We now quantify this argument. The heat influx feeding the corner flow scales as $J_{\mathrm{in}} \sim \kappa \Delta H^{-1}\mathrm{Nu}$. The outflux of thermal and kinetic energy is either of diffusive or of convective origin. We model it as $J_{\mathrm{out}} = J_{\mathrm{out}}^{\mathrm{diff}} + J_{\mathrm{out}}^{\mathrm{conv}}$. Flow reversal is prevented if $J_{\mathrm{out}} > J_{\mathrm{in}}$. The convective outflux, which is dominant for large Pr, is modeled by $J_{\mathrm{out}}^{\mathrm{conv}} \sim J_{\mathrm{in}} \lambda_u / \lambda_\theta \sim \kappa \Delta H^{-1}\mathrm{Nu}^2/\sqrt{\mathrm{Re}}$. The diffusive outflux is $J_{\mathrm{out}}^{\mathrm{diff}} \sim \kappa_t \Delta H^{-1}\mathrm{Nu}$ with some effective, turbulent thermal diffusivity $\kappa_t = \nu_t/\mathrm{Pr} \sim \mathrm{Pr}^{-1}U^4/\epsilon \sim \kappa \mathrm{Pr}^2\mathrm{Re}^4/(\mathrm{NuRa})$, where we have assumed $\mathrm{Pr}_t \approx \mathrm{Pr}$ and employed the k-ϵ model [21] for the turbulent viscosity ν_t.

For dominant diffusive outflux (thus low Pr), suppression of reversals occurs at $\kappa_t \geq \kappa$. The threshold is given by the scaling relation $\mathrm{NuRa} \sim \mathrm{Pr}^2\mathrm{Re}^4$. Inserting Nu(Ra, Pr) and Re(Ra, Pr) either from experiment or from the unifying theory of Refs. [22], one obtains a relation between the critical Prandtl number $\mathrm{Pr}_{\mathrm{crit}}$ and the critical Rayleigh number $\mathrm{Ra}_{\mathrm{crit}}$ at which reversals stop. Depending on whether regime I_u, II_u, or IV_u of Refs. [22] is dominant, we obtain $\mathrm{Pr}_{\mathrm{crit}} \sim \mathrm{Ra}_{\mathrm{crit}}^{\gamma}$, with $\gamma = 3/5$ or $2/3$, respectively, which correctly reflects the trend in Fig. 4.

For large Pr the convective outflux will be dominant. Here the threshold condition is $\kappa \sim \kappa\mathrm{Nu}/\sqrt{\mathrm{Re}}$, which with Nu(Ra, Pr) and Re(Ra, Pr) in regime I_u of Refs. [22] leads to an Ra-independent $\mathrm{Pr}_{\mathrm{crit}}$, beyond which no reversals are possible. The reality of Fig. 4 is clearly more complicated [23], but at least the general trends are consistent with this explanation.

Finally, we note that we also performed experiments and simulations for $\Gamma = 0.85$. Even for this relatively small change in Γ the overall flow dynamics is very different and much more complex as compared to the case of $\Gamma = 1$. Just as the important role the corner flows play for reversals, this finding demonstrates the strong effect of the cell geometry on the overall flow dynamics in the $\Gamma = O(\infty)$ regime. In full 3D geometries, it may be less pronounced, but it certainly is present, too, see also Ref. [24]. It remains remarkably that the rich structure in the (Ra, Pr, Γ) parameter space for reversals is hardly reflected in Nu and Re.

We thank E. Calzavarini for discussions and codeveloping the code. Moreover, we acknowledge support by the Research Grants Council of Hong Kong SAR (No. CUHK403806 and No. 403807) (R. N., S. Q. Z., H. D. X., K. Q. X.), and by the research programme of FOM, which is financially supported by NWO (R. J. A. M. S., D. L.).

*d.lohse@utwente.nl

[1] G. Ahlers, S. Grossmann, and D. Lohse, Rev. Mod. Phys. **81**, 503 (2009).
[2] D. Lohse and K.-Q. Xia, Annu. Rev. Fluid Mech. **42**, 335 (2010).
[3] K. R. Sreenivasan, A. Bershadski, and J. Niemela, Phys. Rev. E **65**, 056306 (2002).
[4] E. Brown and G. Ahlers, J. Fluid Mech. **568**, 351 (2006).
[5] E. Brown and G. Ahlers, Phys. Rev. Lett. **98**, 134501 (2007).
[6] H.-D. Xi and K.-Q. Xia, Phys. Rev. E **75**, 066307 (2007).
[7] H.-D. Xi and K.-Q. Xia, Phys. Rev. E **78**, 036326 (2008).
[8] R. Benzi, Phys. Rev. Lett. **95**, 024502 (2005).
[9] E. Brown and G. Ahlers, Phys. Fluids **20**, 075101 (2008).
[10] C. Resagk *et al.*, Phys. Fluids **18**, 095105 (2006).
[11] F. Fontenele Araujo, S. Grossmann, and D. Lohse, Phys. Rev. Lett. **95**, 084502 (2005).
[12] H. D. Xi *et al.*, Phys. Rev. Lett. **102**, 044503 (2009).
[13] E. Brown and G. Ahlers, J. Fluid Mech. **638**, 383 (2009).
[14] J. Schmalzl, M. Breuer, and U. Hansen, Geophys. Astrophys. Fluid Dyn. **96**, 381 (2002).
[15] K.-Q. Xia, C. Sun, and S.-Q. Zhou, Phys. Rev. E **68**, 066303 (2003).
[16] K. Sugiyama, E. Calzavarini, S. Grossmann, and D. Lohse, J. Fluid Mech. **637**, 105 (2009).
[17] R. J. A. M. Stevens, R. Verzicco, and D. Lohse, J. Fluid Mech. **643**, 495 (2010).
[18] See supplementary material at http://link.aps.org/supplemental/10.1103/PhysRevLett.105.034503 for movies of the flow reversals in the quasi-two-dimensional Rayleigh-Bénard convection for the parameters of Fig. 1.
[19] G. J. F. van Heijst, H. J. H. Clercx, and D. Molenaar, J. Fluid Mech. **554**, 411 (2006).
[20] R. J. A. M. Stevens, H. J. H. Clercx, and D. Lohse, New J. Phys. **12**, 075005 (2010).
[21] S. B. Pope, *Turbulent Flows* (Cambridge University Press, Cambridge, 2000).
[22] S. Grossmann and D. Lohse, J. Fluid Mech. **407**, 27 (2000); Phys. Rev. Lett. **86**, 3316 (2001); Phys. Rev. E **66**, 016305 (2002).
[23] For small Ra and large Pr (upper left corner of the phase diagram Fig. 4) the flow is plume dominated, has a very large coherence length, and no developed rolls exist. However, the angular momentum has zeros.
[24] Z. A. Daya and R. E. Ecke, Phys. Rev. Lett. **87**, 184501 (2001).